





RESEARCH ARTICLE

Protective effect of Cyclo(His-Pro) on peritoneal fibrosis through regulation of HDAC3 expression

Ji Eun Kim¹  | Dohyun Han²  | Kyu Hong Kim³  | Areum Seo⁴  |
 Jong Joo Moon⁵  | Jin Seon Jeong⁶  | Ji Hye Kim⁷  | Eunjeong Kang⁸  |
 Eunjin Bae⁹  | Yong Chul Kim^{5,10}  | Jae Wook Lee¹¹  | Ran-hui Cha¹²  |
 Dong Ki Kim^{5,10}  | Kook-Hwan Oh⁵  | Yon Su Kim^{5,10}  | Hoe-Yune Jung^{13,14}  |
 Seung Hee Yang^{4,10} 

¹Department of Internal Medicine, Korea University Guro Hospital, Seoul, Korea

²Proteomics Core Facility, Seoul National University Hospital, Seoul, Korea

³Department of Biomedical Sciences, Seoul National University Graduate School, Seoul, Korea

⁴Biomedical Research Institute, Seoul National University Hospital, Seoul, Korea

⁵Department of Internal Medicine, Seoul National University Hospital, Seoul, Korea

⁶Department of Internal Medicine, Veterans Health Service Medical Center, Seoul, Korea

⁷Department of Internal Medicine, Chungbuk National University Hospital, Cheongju, Korea

⁸Transplantation Center, Seoul National University Hospital, Seoul, Korea

⁹Department of Internal Medicine, Gyeongsang National University Changwon Hospital, Changwon, Korea

¹⁰Kidney Research Institute, Seoul National University College of Medicine, Seoul, Korea

¹¹Nephrology Clinic, National Cancer Center, Goyang, Korea

¹²Department of Internal Medicine, National Medical Center, Seoul, Korea

¹³R&D Center, NovMetaPharma Co., Ltd, Pohang, Korea

¹⁴School of Interdisciplinary Bioscience and Bioengineering, Pohang University of Science and Technology (POSTECH), Pohang, Korea

Correspondence

Hoe-Yune Jung, R&D Center,
NovMetaPharma Co., Ltd., School
of Interdisciplinary Bioscience and
Bioengineering, Pohang University of
Science and Technology (POSTECH),
394 Jigok-ro, Namgu, Pohang,
Gyeongbuk 37668, Korea.
Email: elijah98@novmeta.com

Seung Hee Yang, Seoul National
University Biomedical Research
Institute and Kidney Research
Institute, Seoul National University,
101 Daehak-ro, Jongno-gu, Seoul 03080,
Korea.
Email: ysh5794@gmail.com

Abstract

Peritoneal dialysis is a common treatment for end-stage renal disease, but complications often force its discontinuation. Preventive treatments for peritoneal inflammation and fibrosis are currently lacking. Cyclo(His-Pro) (CHP), a naturally occurring cyclic dipeptide, has demonstrated protective effects in various fibrotic diseases, yet its potential role in peritoneal fibrosis (PF) remains uncertain. In a mouse model of induced PF, CHP was administered, and quantitative proteomic analysis using liquid chromatography–tandem mass spectrometry was employed to identify PF-related protein signaling pathways. The results were further validated using human primary cultured mesothelial cells. This analysis revealed the involvement of histone deacetylase 3 (HDAC3) in the PF signaling pathway. CHP administration effectively mitigated PF in

This is an open access article under the terms of the [Creative Commons Attribution-NonCommercial-NoDerivs](https://creativecommons.org/licenses/by-nc-nd/4.0/) License, which permits use and distribution in any medium, provided the original work is properly cited, the use is non-commercial and no modifications or adaptations are made.

© 2024 The Author(s). *The FASEB Journal* published by Wiley Periodicals LLC on behalf of Federation of American Societies for Experimental Biology.

Funding information

Seoul National University Hospital (SNUH), Grant/Award Number: 0620190730, 0320190030 and 0411-20190075

both peritoneal tissue and human primary cultured mesothelial cells, concurrently regulating fibrosis-related markers and HDAC3 expression. Moreover, CHP enhanced the expression of nuclear factor erythroid 2-related factor 2 (Nrf2) while suppressing forkhead box protein M1 (FOXO1), known to inhibit Nrf2 transcription through its interaction with HDAC3. CHP also displayed an impact on spleen myeloid-derived suppressor cells, suggesting an immunomodulatory effect. Notably, CHP improved mitochondrial function in peritoneal tissue, resulting in increased mitochondrial membrane potential and adenosine triphosphate production. This study suggests that CHP can significantly prevent PF in peritoneal dialysis patients by modulating HDAC3 expression and associated signaling pathways, reducing fibrosis and inflammation markers, and improving mitochondrial function.

KEYWORDS

Cyclo(His-Pro), dialysis, HDAC3, mitochondria, peritoneal fibrosis

1 | INTRODUCTION

Peritoneal dialysis is a treatment option for end-stage renal disease, showing similar patient prognoses to those of hemodialysis.¹ Even with the various benefits of peritoneal dialysis, including flexibility of time and schedules and better transplant outcomes, several complications often led to withdrawal of peritoneal dialysis.²⁻⁴

Peritonitis is the most common and important complication in peritoneal dialysis patients.⁴ Chronic inflammation related to long-term exposure to high concentration glucose and recurrent bacterial infections cause fibrosing consequences, which are presumed to be associated with various inflammatory protein signaling pathways, such as transforming growth factor-beta (TGF- β), tissue inhibitors of metalloproteinases, and matrix metalloproteinases.⁵⁻⁷ Various complications associated with peritoneal catheters may also lead to progressive peritonitis and fibrosis.⁸

Although the mechanism of peritoneal fibrosis (PF) remains unclear, there is growing evidence that oxidative stress plays a significant role in the pathophysiology of peritoneal membrane damage. Glucose-rich and acidic hypertonic peritoneal dialysis solutions have been specifically implicated in increasing oxidative stress levels.^{9,10} Some treatments targeting oxidative stress appear to modulate peritoneal inflammation and fibrosis.^{11,12} Mitochondria are central to oxidative stress generation, acting as both sources and targets of reactive oxygen species (ROS).¹³ Mitochondrial dysfunction has been identified as a major contributor to glucose-rich dialysate-induced ROS generation, apoptosis, and mitochondrial DNA damage in human peritoneal cells.^{14,15}

Our group recently reported that Cyclo(His-Pro) (CHP), an endogenous cyclic dipeptide that exerts

oxidative damage protection, may have a protective role in chronic kidney disease progression.¹⁶ There is accumulating evidence supporting the protective effects of CHP against oxidative stress and fibrosis in various organs, although the underlying mechanisms remain underexplored.¹⁷⁻²¹ Therefore, the primary objective of this study is to investigate the role of CHP in PF and to elucidate the relevant protein signaling pathways through quantitative mass spectrometry-based proteomics analysis.

2 | MATERIALS AND METHODS

2.1 | Peritoneal fibrosis induction in mice

Eight-week-old B6 male mice were purchased from The Jackson Laboratory (Bar Harbor, ME, USA). All experiments were performed in accordance with the Guidelines for the Care and Use of Laboratory Animals of the National Research Council and the US National Institutes of Health under the approval of the Institutional Animal Care and Use Committee of the Clinical Research Institute at Seoul National University Hospital (Approval no. 20-0061-S1A0). To induce PF, mice in PF and PF with CHP treatment (PF + CHP) groups were injected intraperitoneally with chlorhexidine gluconate (CG) every 3 days for 30 days. For the sham group, an equal volume of 15% ethanol in normal saline was injected in same way. In the PF + CHP group, 17.5 or 35 mg/kg of oral CHP was given by oral gavage once prior to the CG injection. After 30 days all mice were anesthetized via intraperitoneal injection of xylazine and sacrificed to obtain peritoneal tissues.

2.2 | Sample preparation for proteomic analysis

Peritoneal tissue samples were prepared as previously described with some modifications.^{22,23} Briefly, protein extraction was performed using an extraction buffer (4% SDS, 2mM TCEP, and 0.1M Tris pH8.0). After sonication, the samples were incubated at 95°C for 30 min to denature tissue proteins. The extracted proteins were precipitated by adding chilled acetone at a buffer to acetone volume ratio of 1:5, followed by incubation at −20°C for 16 h. The protein (50 µg per sample) was digested following the filter-aided sample preparation procedure (FASP) as previously described.²³ Briefly, the precipitated protein samples were dissolved in 50 µL of SDT buffer (4% SDS, 10mM tris(2-carboxyethyl)phosphine (TCEP), and 50mM CAA in 0.1M Tris HCl pH8.5), protein samples were loaded onto a 30K amicon filter (Millipore, Billerica, MA, USA), and the buffer was exchanged with a UA solution (8M UREA in 0.1M Tris-HCl pH8.5) via centrifugation at 14000g. Following further buffer exchange employing 40mM ammonium bicarbonate (ABC), protein digestion was performed overnight at 37°C using a trypsin/LysC mixture (enzyme to substrate ratio of 1:100). The resulting peptides were collected to new Eppendorf tubes via centrifugation, and an additional elution step was sequentially performed using 40mM ABC and 0.5M NaCl. All peptides were acidified with 10% trifluoroacetic acid (TFA; Thermo Fisher Scientific, Waltham, MA, USA). Thereafter, a three-fractionation strategy was applied to increase the proteome depth. The acidified peptides were loaded in homemade sulfonated styrene-divinylbenzene polymer (SDB-RPS) StageTips (3M, St. Paul, MN, USA), following previously described procedures.²⁴ Fractionated peptides were completely dried with a vacuum dryer and stored at −80°C.

2.3 | Library sample preparation

For the peritoneal tissue proteome library, 100 µg of peptide from pooled tissue sample was fractionated by with Agilent 1260 HPLC (Agilent, Santa Clara, CA, USA) as described procedures.²⁵ In brief, the samples were dissolved in 90 µL of buffer A (10mM ammonium formate solution, pH10, with 2% acetonitrile) and loaded on a ZORBAX 300 Extend-C18 column (Agilent, Santa Clara, CA, USA). We collected the sample with 24 fractions by increasing gradients of buffer B (15mM ammonium formate solution, pH10, with 2% acetonitrile) from 5% to 40% over 40 min and total run time was 1 h. The 24 fractionated samples were completely dried and stored at −80°C until MS analysis.

2.4 | LC-MS/MS analysis for proteomics

All LC-MS/MS analyses were conducted using an Ultimate 3000 UHPLC system (Dionex, Sunnyvale, CA, USA) coupled with a Q-Exactive HF-X mass spectrometer (Thermo Scientific, Hamburg, Germany) as previously described with some modifications.²⁶ The peptides prepared as described above were resuspended in 2% ACN and 0.1% formic acid and spiked with the HRM kit (Biognosys AG, Schlieren-Zurich, Switzerland) according to the manufacturer's instructions. Peptide samples were separated on a two-column system with a trap column (300 µm I.D × 5 mm length) and an analytical column (EASY-Spray C18, 75 µm I.D × 50 cm length) with a 90-min gradient from 8% to 30% acetonitrile at 300 nL/min. The column temperature was maintained at 60°C using a column heater. A MS1 scan (350–1650 *m/z*) was acquired with a resolution of 70 000 at *m/z* 200. A top-15 method was used to select the precursor ion with an isolation window of 1.2 *m/z*. The MS/MS spectrum was acquired at an HCD-normalized collision energy of 28 with a resolution of 17 500 at *m/z* 200. The maximum ion injection times for the full and MS/MS scans were 20 and 100 ms, respectively.

2.5 | Data processing for label-free quantification

All MS raw files were processed by using interface of MaxQuant (version 1.6.1.0).²⁷ MS/MS spectra were searched from the mouse UniProt protein sequence database using the Andromeda search engine.²⁸ Primary searches were done using a 6-ppm precursor ion tolerance. The MS/MS ion tolerance of 20 ppm was used. Carbamido-methylation of cysteine was specified as the control modification, and N-acetylation of protein and oxidation of methionine were considered as variable modifications. Enzyme specificity was set to full tryptic digestion. Peptides with a minimum length of six amino acids and up to two missed cleavages were included. The acceptable false discovery rate (FDR) was set to 1% at the peptide, protein, and modification levels. To maximize quantification events across samples, we enabled the “Match between Runs” option of the MaxQuant platform. LFQ was performed with a minimum ratio count of one.²⁹

2.6 | Peritoneal histology and Immunohistochemistry

Peritoneum were fixed in 4% phosphate-buffered paraformaldehyde (Huarui Scientific and Technological Co.) for 12–24 h and then embedded in paraffin for light

microscopy examination. Tissue sections of 4 μ m thickness were stained for periodic acid-Schiff base staining for morphological evaluation, and Masson's trichrome and Sirius Red were used to assess the degree of fibrosis.

The paraffin-embedded sections were deparaffinized with xylene and dehydrated in ethanol. For immunohistochemical analysis, the dehydrated tissue sections were stained according to the instructions in the kit. Primary antibodies were as follows: anti-pP65 (1:100, Santa Cruz, sc-136548), anti-ColA1 (1:200, Santa Cruz, sc-293182), anti-pHDAC3 (1:200, Cell Signaling Technology, 3815S), anti-Sod-1 (1:200, Aviva System Bio, OABB00304), ICAM-1 (1:200, Abcam, ab-171123), anti-8-OHdG (1:300, Abcam, ab-48508), anti-F4/80 (1:100, Cell Signaling Technology, 70076S), anti-p21 (1:200, Santa Cruz, sc-6246), anti-fibronectin (1:200, Santa Cruz, sc-18825), anti-cytochrome C (1:200, Thermo Fisher Scientific, MA5-11674), anti-TGF- β (1:200, Santa Cruz, sc-373936), anti-Nrf2 (1:100, Proteintech, 16396-1-AP), and anti-FOXM1 (1:200, Proteintech, 13147-1-AP). Immunohistochemical images were captured using a Leica inverted light microscope (Leica Camera, Wetzlar, Germany). The degree of fibrosis and the positive area of primary antibodies for five fields was scored quantitatively using the LAS-4000 program (Leica Camera, Germany).³⁰

2.7 | Flow cytometry

A mouse spleen was placed into a cell strainer over a 50 mL conical tube. The spleen tissue was gently disintegrated by applying pressure through the plunger of a syringe and subsequently rinsed with 1 \times PBS through the 40 μ m strainer. The isolated splenocytes were carefully suspended in 1 \times Red Blood Cell Lysis buffer and incubated at room temperature for 10 min. Afterward, cells were washed with 1 \times PBS and collected in 5 mL polystyrene tubes (BD Biosciences, CA, USA) using Hank's Balanced Salt Solution-based FACs buffer (HBSS; 5% BSA and 0.5% sodium azide). In the FACs experiment, the cells were stained with fluorescence-conjugated mouse antibodies anti-CD45 (APC, BD Biosciences, 559864), anti-Gr-1 (BV421, Biolegend, 108433), anti-F4/80 (PE, Biolegend, 157304), and anti-CD11b (FITC, Biolegend, 101206). The cells' viability, apoptosis, and necrosis were measured using an Annexin V/propidium iodide (PI) fluorescence isothiocyanate (FITC) apoptosis kit (BD Biosciences, NJ, USA). Before proceeding, HPMCs were pretreated either with recombinant TGF- β (rTGF- β , 1 ng/mL) for a duration of 24 h or with H₂O₂ (0.5 mM) for 1 h. Subsequently, the cells were

resuspended in 100 μ L of binding buffer and incubated for 15 min in the dark. Thereafter, 5 μ L FITC-conjugated Annexin V (10 mg/mL) and 5 μ L PI (50 mg/mL) was added for cell staining. Data were acquired and analyzed using the BDCanto (FACSDiva ver. 80; BD Biosciences) and further analyzed with FlowJo software (version 10.0.7; FlowJo LLC, Ashland, OR, USA).

2.8 | Western blot analysis

The total protein of peritoneal tissue and primary cultured cells was extracted using radioimmunoprecipitation assay lysis buffer containing the Halt protease inhibitor (Pierce, Rockford, IL, USA). Western immunoblotting was performed using primary antibodies against fibronectin (Sc-6952), Collagen 1A (Sc8784), α SMA (Abcam, Ab5694), p16 (LSBio, LS-b5261), p21 (Santa Cruz, Sc-6246), pHDAC3 (Cell Signaling Technology, 38155), and GAPDH (Cell Signaling Technology, 2118). Briefly, the proteins were loaded onto 8%–12% sodium dodecyl sulfate-polyacrylamide gels and transferred onto Immobilon-FL 0.4 μ m polyvinylidene difluoride membranes (Millipore, Billerica, MA, USA). After blocking with 5% BSA, the membranes were incubated with each primary antibody. The membranes were then incubated with anti-rabbit IgG (Cell Signaling Technology) and anti-mouse IgG (Cell Signaling Technology) for 1 h at room temperature. The immunoblot bands were visualized and captured using an Image Quant LAS 4000 mini (GE Healthcare, Piscataway, NJ, USA). Quantification of band intensity was analyzed by ImageJ (National Institutes of Health, Bethesda, MD, USA).

2.9 | Real time qPCR

Total RNA was extracted from the peritoneum and cells, and the target gene mRNA levels were assessed by real-time qPCR as previously described.³¹ All primers for real-time qPCR are listed in Table S1. In brief, total RNA was extracted from the peritoneal tissue or HPMCs using the RNeasy kit (Qiagen GmbH, Hilden, Germany), and 500 ng total RNA was reverse transcribed using oligo-d(T) primers and AMV-RT Taq polymerase (Promega, Madison, WI, USA). Real-time qPCR was analyzed with primers for *FN1*, *Col1A1*, *α -SMA*, *Bax*, *p53*, *p21*, *OGG-1*, *HDAC3*, *FOXM1*, *NRF2*, and *GAPDH* (Applied Biosystems, Foster City, CA, USA) in triplicate for each sample. Relative quantification, mRNA/GAPDH mRNA ratio, was determined by the formula $2^{-\Delta\Delta CT}$.

2.10 | Preparation of primary cultured human mesothelial cells and fibrosis induction in cells

For the validation analysis for the significant protein we found in proteomics analysis, we used HPMC. We collected dialysis effluent from the clinically stable peritoneal dialysis patients. HPMCs were harvested and cultured from the dialysis effluent, as mentioned in our previous study.³² In brief, the effluent in bags were suspended for 3–4 h in an incubator to settle the cells at the bottom of the effluent. The settled cells were transferred to 50 mL tubes to centrifuge at 1500 rpm for 20 min and washed with phosphate-buffered saline. The cell pellets were re-suspended in culture medium and seeded in 25 cm² tissue culture flasks and incubated. We used culture medium contains M199 (Biological Industries) supplemented with 20% fetal bovine serum, 100 IU/mL penicillin, 100 mg/mL streptomycin, and 2% Biogro-2 (Biological Industries), which contains insulin, transferrin, ethanolamine, and putrescine. The second passage of HPMC was used for the further analysis.

PF was induced in primary cultured HPMCs with 1 ng/mL rTGF- β (R&D Systems). To find the effect of CHP on fibrosis status as well as the protein we found to be related with PF, the HPMCs were simultaneously treated with 0.5, 1, or 2 μ g/mL of CHP (NovMetaPharma Co., Ltd).

2.11 | Immunofluorescence staining

Immunofluorescence staining was conducted on peritoneal tissues and human primary cultured mesothelial cells (HPMCs) using specific antibodies. In vivo, deparaffinized peritoneal sections were probed with the following antibodies: DAPI (1:1000; Thermo Fisher Scientific, 62248), pHDAC3 (1:100; Cell Signaling Technology, 3815), and FOXM-1 (1:100; Santa Cruz, sc-271746). In vitro, HPMCs were incubated with PBS-diluted antibodies against DAPI (1:1000; Thermo Fisher Scientific, 62248), fibronectin (1:100; Santa Cruz, sc-8422), and pHDAC3 (1:100; Cell Signaling Technology, 3815) at 4°C overnight. Subsequently, Alexa Fluor 488 (1:400; Thermo Fisher Scientific, A-10631) and Alexa Fluor 555 (1:400; Thermo Fisher Scientific, A-21433) were added at room temperature for 30 min.

The immunofluorescence staining was visualized using a confocal microscopy system equipped with a Leica TCS SP8 STED CW (Leica Microsystems). Automatic image analysis was performed using MetaMorph v.7.8.10 software (Universal Imaging, Nashville, TN).

2.12 | Transmission electron microscopy for ultrastructural analysis

Small pieces (1 mm³) of the peritoneal layer were fixed with 2.5% glutaraldehyde (Sigma-Aldrich) at 0°C for 2 h, subsequently post-fixed in 1% osmium tetroxide, and then washed in distilled water. The fixed samples were incubated on uranyl acetate for 1 h, followed by dehydration with graded ethanol and 100% propylene oxide treatments. For transmission electron microscopy imaging, ultrathin sections (70 nm) were cut on the ultramicrotome, mounted on formvar-coated grids, and stained with lead citrate. Images were acquired from five randomly selected areas within three different glomeruli of the mouse peritoneal layers using a JEM-1400 electron microscope (JEOL Ltd., Akishima, Tokyo, Japan).

2.13 | Assessment of Mitochondrial Membrane Potential

Mitochondrial membrane potential ($\Delta\Psi$) in response to renal fibrosis induced by rTGF- β (2 ng/mL) was evaluated using the MitoProbe JC-1 Assay kit (Invitrogen, US). Specifically, the cells were incubated for 24 h, followed by treatment with JC-1 (10 μ L of 200 μ M) at 37°C for 30 min, according to the manufacturer's instructions. A decrease in mitochondrial depolarization patterns of cells was then examined and photographed using an inverted fluorescent microscope Lecia TCS SP8 (Lecia, Germany) and quantified using CLSM Analysis Software LAS-X (Lecia, Germany) imaging software.

2.14 | Measurement of oxygen consumption rate and extracellular acidification rate

Oxygen consumption rate (OCR) and ECAR were measured using a Seahorse XF adenosine triphosphate Real-Time rate assay (Agilent Technologies, CA, US). Specifically, HPMCs with H₂O₂ (0.5 mM) and CHP (0.5 μ g/mL) were seeded on a seahorse plate and placed in the hood for 1 h. Then the cells were washed with XF assay media, after which 450 μ L XF assay media were added to each well. Following equilibration for 20 min, each well of the plate was sequentially injected with oligomycin (2 μ g/mL), carbonyl cyanide 3-chlorophenylhydrazone (5 μ M), and rotenone (2 μ M). OCR and ECAR were measured and analyzed using “wave” software from Seahorse (Agilent Technologies).

2.15 | Human peritoneal fluid collection

This study was approved by the Medical Ethics Committee of the Seoul National University Hospital (institutional review board [IRB] number: H-1506-097-681) and complied with the Declaration of Helsinki. This study included only participants who provided informed consent and agreed to provide PF samples. We collected PF from 31 patients on maintenance peritoneal dialysis without evidence of peritonitis to measure CHP levels in PF.

2.16 | Measurement of CHP in peritoneal fluid

The CHP content in peritoneal fluid was measured by Q-Exactive Orbitrap hybrid mass spectrometer (Thermo Fisher Scientific) along with an Agilent 1290 LC system (Agilent Technologies) after extraction with methanol. Each volume of samples was adjusted by 100 µg of peritoneal fluid protein concentration analyzed using a bicinchoninic acid assay (Thermo Fisher Scientific). The final concentration of the internal standard was 100 µg/mL (IS, L-proline-2,5,5-d₃), which was then diluted by adding three times that volume of chilled methanol to the sample. L-proline-2,5,5-d₃ was purchased from Sigma-Aldrich (St. Louis, MO, USA). Peritoneal fluid samples were vortex mixed, centrifuged, and then the organic phase was evaporated to dryness using SpeedVac. The residue was reconstituted in 100 µL of 0.1% formic acid and injected 5 µL into the LC-MS/MS system. The calibration curve was linear over the range of 0.1–1000 ng/mL with the coefficients of correlation (*r*) greater than 0.99 in all instances. The lower limit of quantification of CHP was 0.1 ng/mL. The analyte and IS were separated on a Hypersil Gold (150 × 2.1 mm, 5 µm, Thermo, USA) under gradient conditions. The mobile phases consisted of 0.1% formic acid in distilled water and 80% acetonitrile in formic acid. The gradient of the mobile phase was as follows: 1% solvent B in 1.5 min, 1%–8% solvent B in 10.5 min, 8%–15% solvent B in 3 min, 15%–30% solvent B in 4 min, 30%–80% solvent B in 4.4 min, and 80%–1% solvent B for 6.6 min. The electrospray ionization source was set up as follows: positive mode, spray voltage of 2.8 kV, and capillary temperature of 320°C. Properties of Full MS/dd-MS2 were set up as follows: full-MS scans, 100–1000 *m/z* of scan range, 70 000 of resolution at 400 *m/z*, 1 × 10⁶ of AGC target, and maximum injection time (IT) of 60 ms. MS2 scans used the following parameters: 17 500 of resolution at 400 *m/z*, 2 × 10⁵ of AGC target, maximum IT of 250 ms, ±2 *m/z* of isolation width, 90 s of a dynamic

exclusion time, and normalized collision energy (NCE) for dd-MS2 of 30%.

2.17 | Statistical analysis

Statistical analyses for proteomic data were performed using Perseus software.³³ Initially, proteins were only identified when site, reverse, and contaminants were removed. The expression level of proteins was estimated by determining their LFQ values calculated from MaxLFQ algorithm in Maxquant software.²⁹ Because of the skewed distribution of the data, log₂ transformation was conducted for these values. Valid values were filtered with proteins with a minimum of 60% quantified values in at least one sample group. Missing values were included based on a normal distribution (width=0.3, down-shift=1.8) to simulate signals of low-abundance proteins. Two-sided *t*-tests were performed for pairwise comparison of proteomes to detect DEPs. The protein abundances were subjected to z-normalization followed by hierarchical clustering with Pearson's correlation distance. Principle component analysis was performed using Perseus software.

For the comparison of mRNA levels between groups, the Kruskal–Wallis test was used. GraphPad Prism 8.0 software (Graph Pad, Inc., La Jolla, CA, USA) was used for the statistical analysis and constructing the bar plots.

2.18 | Bioinformatics analysis

Canonical pathway enrichment and upstream regulator prediction were performed via Ingenuity Pathway Analysis (IPA, QIAGEN, Hilden, Germany) based on DEPs in the peritoneal tissue experiments. The statistical significance of both the gene ontology classification and enrichment analysis was determined by Fisher's exact test. All statistical tests were two-sided, and *p* < .05 was considered statistically significant.

3 | RESULTS

3.1 | Effect of CHP on PF in mice

To gain insight into the role of CHP in PF, we generated a PF murine model by inducing inflammation by injecting CG. Significant increases in collagenous compact zone thickness were observed in the PF group

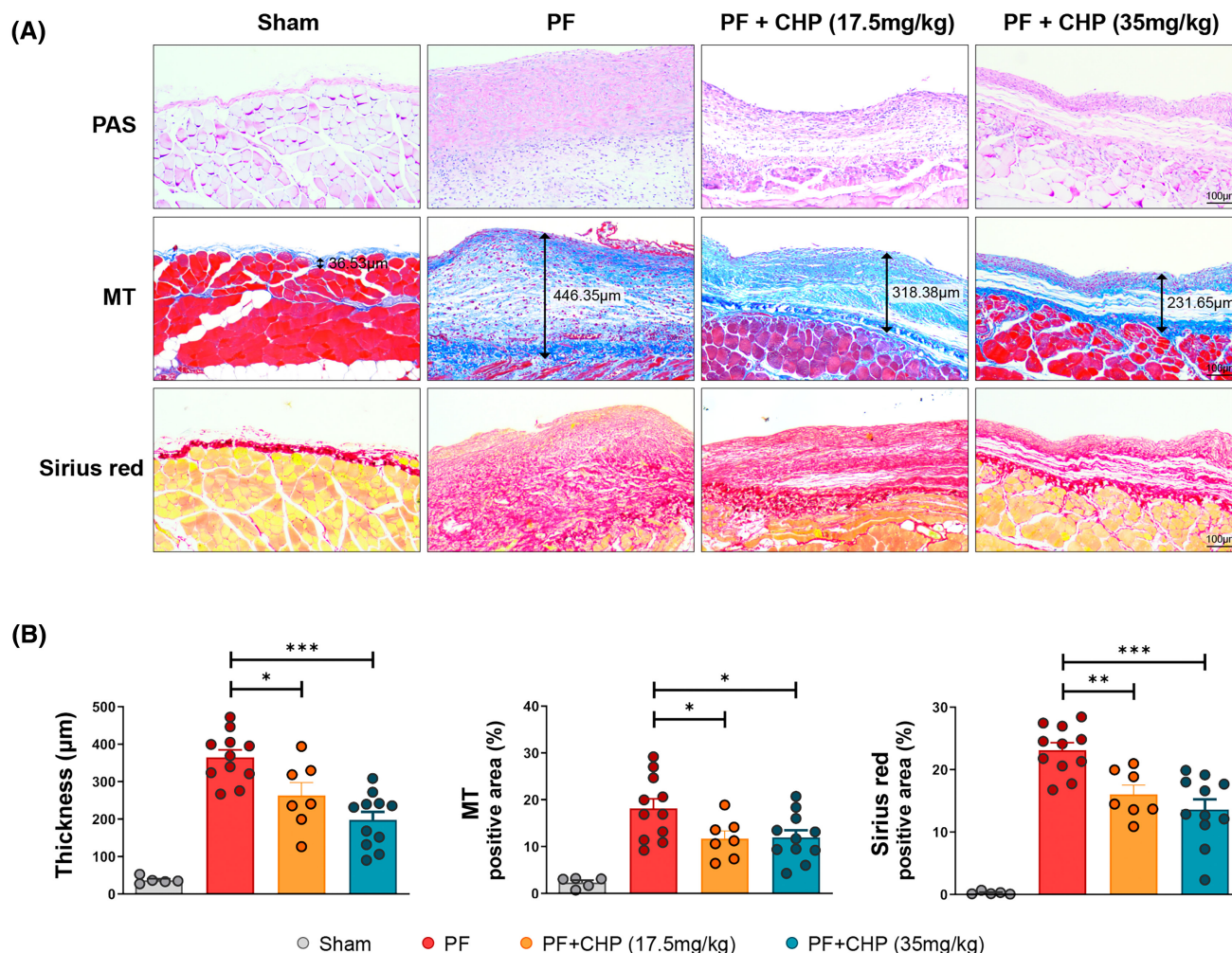


FIGURE 1 Cyclo(His-Pro) (CHP) ameliorates peritoneal fibrosis induced by chlorhexidine gluconate. (A) Morphological change of the peritoneal membrane with or without CHP in Masson's trichrome, Sirius red, and H&E stain. Original magnification, $\times 200$. (B) Quantitative bar plots showing peritoneal thickness, Masson's trichrome stain area, and Sirius red stain area in the Sham, PF, and PF + CHP groups. Error bars represent standard error. $*p < .05$; $**p < .01$; $***p < .001$. PD, chlorhexidine gluconate-induced peritoneal dialysis; PF + CHP, CHP-treated PF model.

(Figure 1). Low-dose and high-dose CHP significantly reduced peritoneal thickening in a dose-dependent manner (Figure 1).

3.2 | CHP suppressed inflammatory cytokines in the PF model

To investigate the effect of CHP on fibrosis-related inflammatory molecules, immunohistochemistry (IHC) staining on mouse peritoneal tissue was performed in fibronectin, collagen 1A, TGF- β , intracellular adhesion molecule-1 (ICAM-1), F4/80, and pP65 (Figure 2A). The IHC analysis showed that staining intensity of pro-inflammatory and profibrotic molecules in peritoneum was elevated in PF group, and this elevation was

mitigated by both low- and high-dose CHP treatments (Figure 2B). To further validate these findings, we conducted Western blot (WB) analysis for fibronectin, collagen 1A, TGF- β , ICAM-1, and pP65, which confirmed the results observed in the IHC (Figure 2C). Considering findings that F4/80 staining, which is a marker of mouse monocytic myeloid-derived suppressor cells (MDSCs), in the peritoneum was changed by CHP, we investigated whether CHP changes the population of MDSCs in the spleen after induction of PF. We found that the proportions of three subsets of MDSC populations for CD11b⁺Gr-1⁺, F4/80⁺Gr-1⁺, and CD11b⁺F4/80⁺ were significantly decreased after being treated with a low dose of CHP (17.5 mg/kg) (Figure 2D,E). MDSCs are observed in many pathological conditions, such as intraocular inflammatory disease³⁴ and inflammatory

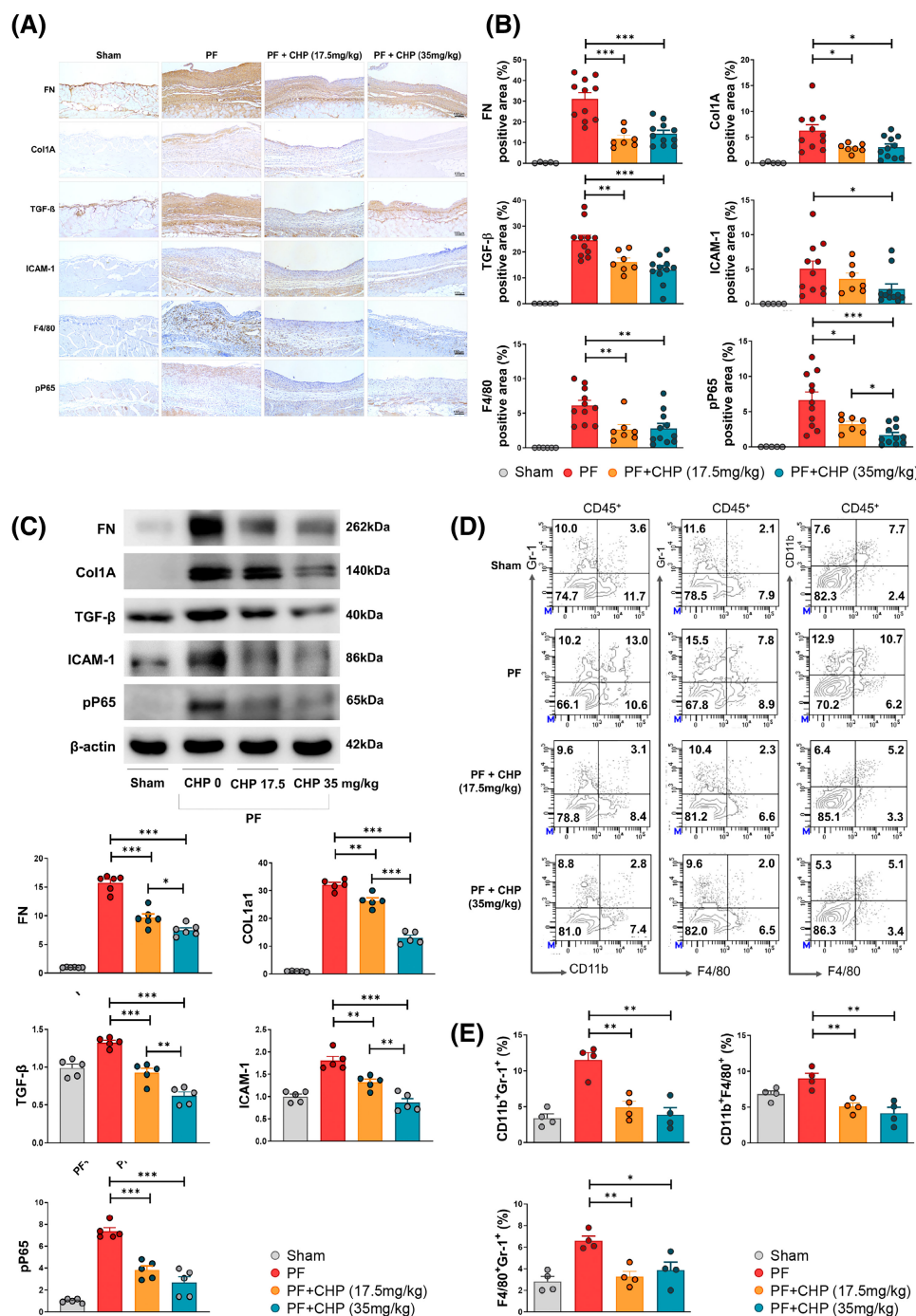


FIGURE 2 Changes of fibrosis and inflammatory markers in peritoneal fibrosis with CHP treatment. (A) Representative images staining for fibrosis markers including fibronectin, collagen 1A and TGF-β as well as inflammation markers such as ICAM-1, F4/80, and pP65 in peritoneal tissues from sham, PF, and PF + CHP. (B) Semiquantitative immunostaining scores of each protein. (C) Representative Western blot and quantitative analysis for fibronectin, collagen 1A, TGF-β, and ICAM-1 in peritoneal tissues from sham, PF, and PF + CHP. (D) Representative flow plots and (E) summary of myeloid cell proportions in the spleen. * $p < .05$; ** $p < .01$; *** $p < .001$.

bowel disease,³⁵ and are also found to suppress T-cell function in model of traumatic stress.³⁶ Our results demonstrate that CHP treatment lead to a reduction in MDSC numbers in PF model, indicating the immunomodulatory effects of CHP in the pathophysiology of peritoneal injury.

3.3 | Proteomic profiling to identify pathways related to the protective effect of CHP on PF

Regarding the notable reduction of PF due to treatment with CHP, a quantitative proteomics analysis was

performed using the peritoneal tissues from the Sham, PF, and PF + CHP groups to discover possible pathways by which CHP treatment ameliorates fibrosis. In the proteomics analysis, over 2000 proteins were identified in each peritoneal tissue sample (Figure 3A). The composition of peritoneal protein was clearly discriminated into groups (Figure 3B). In pairwise comparison between the Sham versus PF and Sham versus PF + CHP

groups, 418 and 661 differentially expressed proteins (DEPs) were discovered, respectively (Figure 3C). In addition, clustering analysis with the Sham, PF, and PF + CHP groups were performed to assess the trend of DEPs by the three groups. We found 33 proteins that increased during peritoneal dialysis but decreased after CHP treatment, as well as 25 proteins which decreased during PF but were elevated after CHP treatment

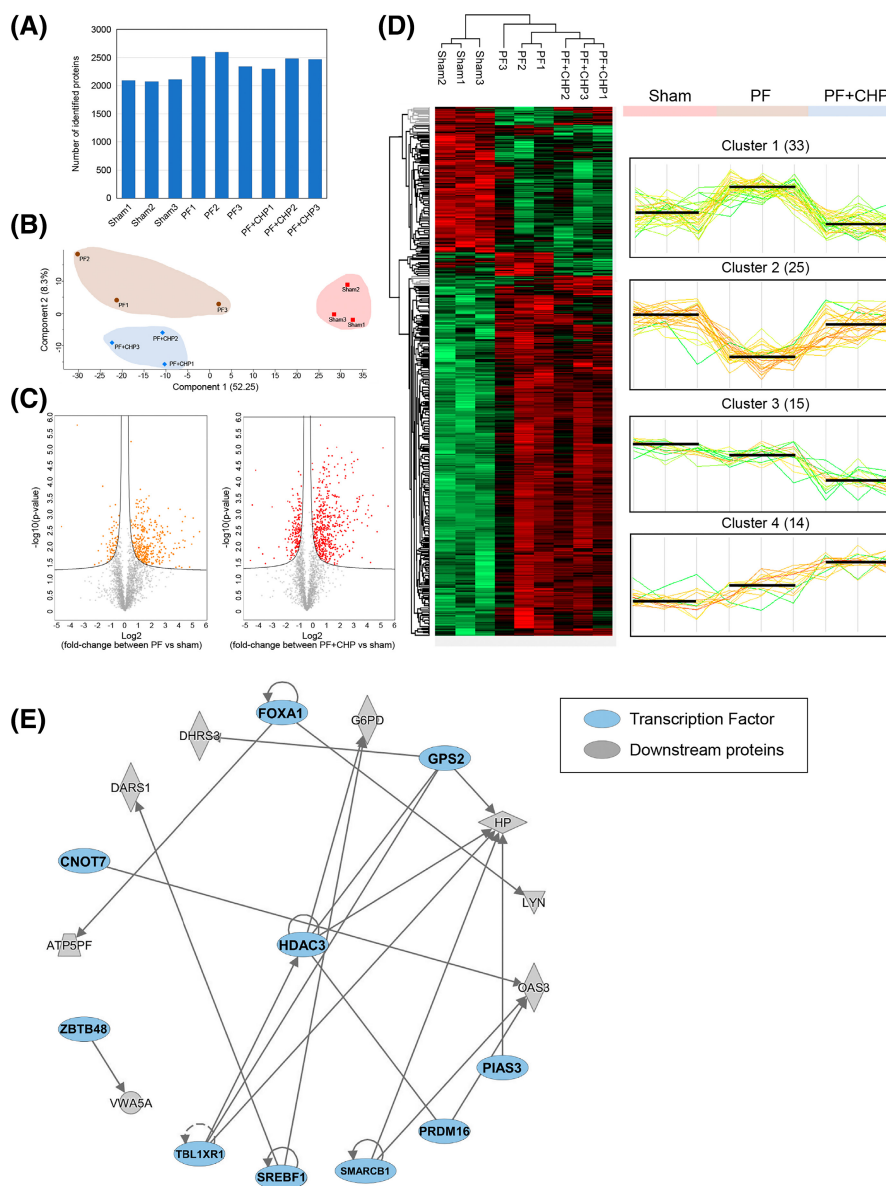


FIGURE 3 Proteomics analysis assessing differentially expressed proteins in sham, PF, and PF + CHP. (A) Identified proteins in each peritoneal tissue sample. (B) Composition of each group shown in principal coordinates analysis. Red, brown, and blue dots represent sham, PF, and PF + CHP groups, respectively. The plot displays PC1 on the x axis and PC2 on the y axis. (C) Volcano plots represent 418 and 661 differentially expressed proteins in PF (left) and PF + CHP (right) groups, respectively, compared with sham. X-axis represents log₂-transformed fold change between groups and y-axis represents -log₁₀ (p-value). (D) Hierarchical clustering analysis showed four major clusters in three groups. Cluster 1 showed elevated expression of fibrosis, which decreased after CHP treatment. Cluster 2 showed the opposite pattern to cluster 1. (E) Upstream regulatory proteins related to differentially expressed proteins in cluster 1. Blue and gray colored proteins represent the predicted upstream regulators (transcription factors) and observed downstream proteins, respectively.

(Figure 3D). In the upstream regulator analysis of DEPs, we identified histone deacetylase 3 (HDAC3), a well-known profibrotic protein, as a common regulator (Figure 3E). Therefore, we further explored the changes of HDAC3 associated with fibrosis and CHP in subsequent analyses.

3.4 | HDAC3 expression was elevated in PF as with other tissue injury markers and alleviated by CHP

To further elucidate the role of CHP associated with HDAC3 in reducing peritoneal injury, IHC staining with HDAC3 and other tissue injury markers were performed. We found increased staining intensities for oxidative stress and apoptosis markers such as cytochrome C, P21, and 8-hydroxy-2'-deoxyguanosine (8-OHdG) in the PF peritoneum, concomitant with increased expression of phospho-HDAC3, all of which were reduced by CHP treatment. Conversely, antioxidant-related proteins including nuclear factor erythroid 2-related factor 2 (Nrf2) and superoxide dismutase 1 (SOD-1) were significantly decreased in PF and restored with CHP treatment (Figure 4A,B).

HDAC3 is known to form complexes with transcriptional cofactors that regulate gene promoters. Forkhead box protein M1 (FOXM1), one of these cofactors, binds to HDAC3 and is involved in the transcriptional repression of Nrf2. In our confocal microscopy examinations, we observed concurrent upregulation of HDAC3 and FOXM1 in the peritoneum of the PF group, and this upregulation was alleviated in both the low- and high-dose CHP treatment groups (Figure 4C).

Similar results were obtained in qPCR assay, which indicated that CHP alleviated the expression of HDAC3 as well as oxidative stress markers and increased expression of Nrf2 after fibrotic injury. FOXM1 expression also increased with peritoneal injury and recovered with CHP co-treatment (Figure 4D). Western blot analysis of peritoneal tissues in the three groups also gives evidence of consistent changes in phospho-HDAC3 with various fibrosis and cell senescence markers, including fibronectin, collagen 1A, α SMA, p16, and p21, in response to PF and CHP treatment (Figure 4E).

3.5 | CHP alleviates the expression of HDAC3 and fibrosis markers, which increased with rTGF- β -induced injury in human primary cultured peritoneal mesothelial cells

We next sought to validate the in vitro role of CHP on peritoneal cell injury. We induced fibrotic injury on human

primary cultured peritoneal mesothelial cells (HPMCs) by recombinant rTGF- β treatment. HPMCs treated with rTGF- β obtained spindle-fibroblastic morphology, but co-treatment with CHP resisted morphological change (Figure 5A). Immunofluorescence analysis showed that fibronectin and pHDAC3 staining intensity in HPMCs was elevated after rTGF- β treatment, and was decreased by CHP treatment (Figure 5B). In consistent with in vivo analyses, mRNA expression of HDAC3, FOXM1, and multiple profibrotic factors were significantly elevated with rTGF- β induction and decreased with CHP treatment in HPMCs (Figure 5C). Furthermore, the degree of amelioration of increased phospho-HDAC3 and fibronectin expression by rTGF- β induction was dose-dependent through CHP treatment (Figure 5D).

3.6 | CHP restored the structure of mitochondria after PF as well as oxidative stress

Considering our findings that multiple mitochondria-related factors, such as Bax and cytochrome C were involved, we next explored mitochondrial changes in oxidative stress as well as fibrotic injury following CHP treatment. We observed the mitochondrial morphology using transmission electron microscopy and found the peritoneal cells from PF mice exhibited a significant decrease in cristae density, indicative of decreased mitochondrial fitness. CHP treatment in PF mouse recovered mitochondrial and cristae morphology (Figure 6A). We then evaluated the in vitro effect of CHP on mitochondrial membrane potential using confocal microscopic analysis of JC-1 staining (Figure 6B). rTGF- β treatment on HPMCs induced depolarization of the mitochondrial membrane potential, as indicated by enhanced JC-1 staining, and this depolarization was restored by CHP co-treatment (Figure 6C). Along with the mitochondrial damage, the viability of HPMCs was considerably decreased after rTGF- β treatment, and this change was markedly recovered by CHP (Figure 6D,E).

Hydrogen peroxide (H_2O_2)-induced injury to HPMCs was used to investigate the effect of CHP on oxidative stress. Treatment with H_2O_2 for 1 h inhibited mitochondrial respiration in HPMCs, which was restored after CHP treatment (Figure 6F). Similarly, the extracellular acidification rate (ECAR), which reflects intracellular lactate production, decreased after H_2O_2 treatment, and increased with CHP cotreatment (Figure 6G). In addition, the apoptotic cell proportion was analyzed by Annexin V-FITC/PI-staining after H_2O_2 and CHP treatment (Figure 6H). In contrast to the significantly increased necrotic cell ratio after H_2O_2 treatment, the necrotic cell ratio decreased, and the

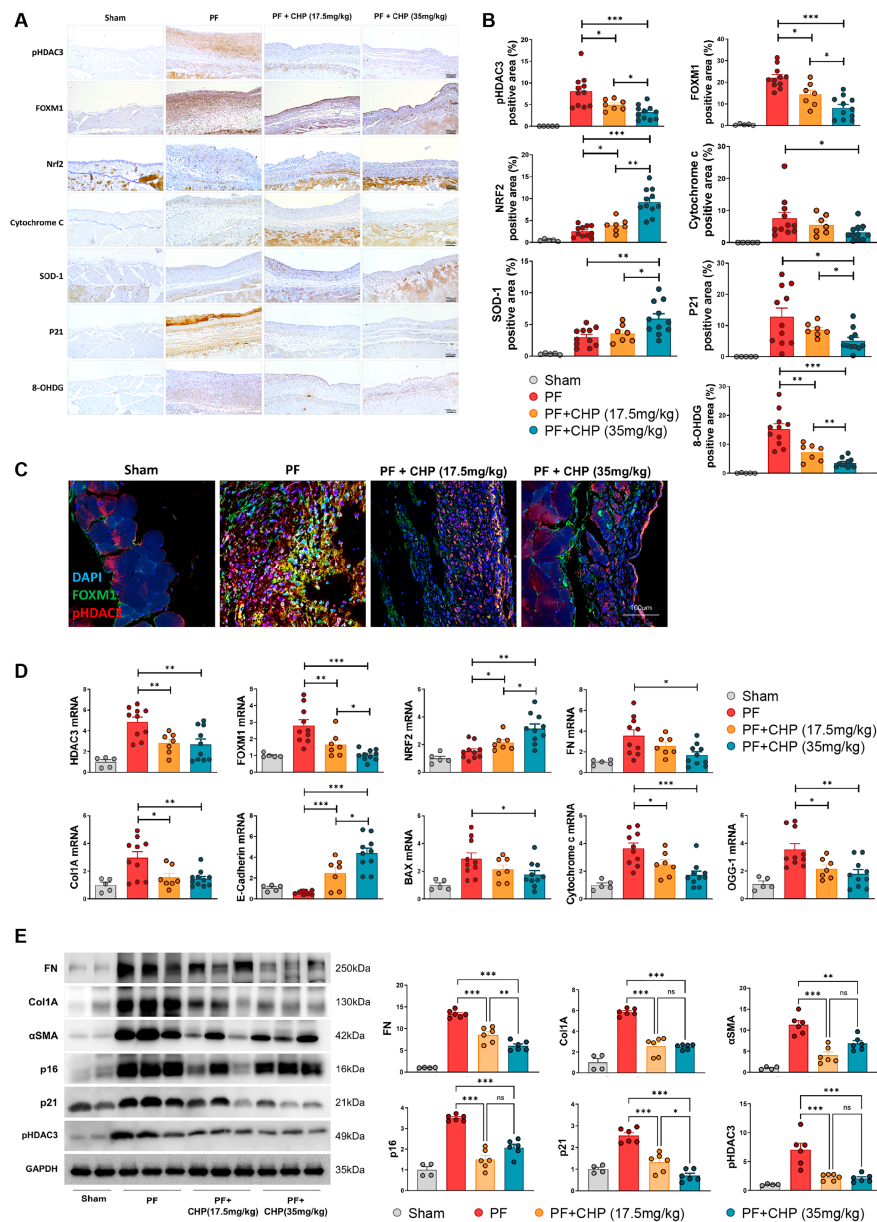


FIGURE 4 pHDAC3 expression with other tissue injury markers in peritoneal tissue after fibrotic injury with and without CHP treatment. (A) Representative images and (B) semiquantitative immunostaining scores for pHDAC3, Nrf2, cytochrome C, SOD-1, P21, and 8-OHdG in peritoneal tissues from sham, PF, and PF + CHP. * $p < .05$; ** $p < .01$; *** $p < .001$. (C) Overlaid confocal fluorescence microscopy images of peritoneal tissues, showing blue fluorescence for DAPI-stained nuclei, red fluorescence related to pHDAC3 and green fluorescence related to FOXM1 (magnification, x400). (D) mRNA expression of HDAC3, FOXM1, and NRF2 as well as other tissue injury markers in each group. Error bars represent standard error. * $p < .05$; ** $p < .01$. (E) Representative blots (upper) and quantitative analysis of band intensities from Western blot analysis (lower) for FN, Col1A, αSMA, p16, p21, and pHDAC3. The experiments were independently repeated three times. * $p < .05$. pHDAC3, phospho-histone deacetylase 3; FOXM1, forkhead box protein M1; NRF2, nuclear factor (erythroid-derived 2)-like 2; SOD-1, superoxide dismutase 1; 8-OHdG, 8-hydroxy-2'-deoxyguanosine; FN, fibronectin; Col1A, type 1 collagen; αSMA, alpha-smooth muscle actin.

early apoptotic cell ratio increased in a dose-dependent manner after CHP treatment. This indicates that CHP may delay or inhibit cell death in response to oxidative stress injury (Figure 6I). Collectively, these results indicate that CHP may restore the reduced mitochondrial respiration and glycolysis induced by oxidative stress, which inhibits cell death in the chronic phase.

3.7 | CHP levels in human peritoneal fluid are associated with adequacy of dialysis

We next sought to evaluate CHP levels in the peritoneal fluid of maintenance dialysis patients ($n = 40$). Upon comparing the clinical characteristics of peritoneal

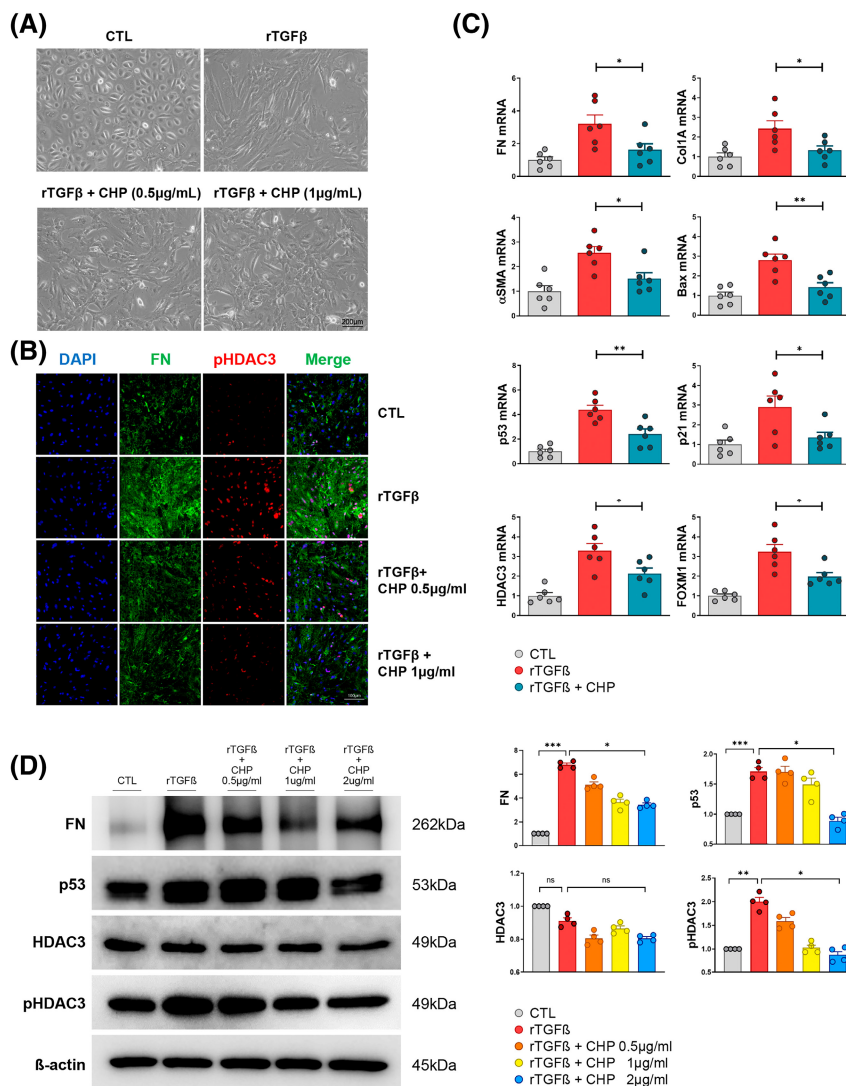


FIGURE 5 Fibrosis in primary cultured mesothelial cells induced by recombinant TGFβ treatment was alleviated by CHP.

(A) Representative image of morphological changes induced 24 h after the introduction of rTGF-β to human primary cultured peritoneal mesothelial cells (HPMCs). HPMCs cultured in the control medium (upper left), medium containing 1 ng/mL of rTGF-β (upper right), and medium containing 1 ng/mL of rTGF-β with 0.5 μg/mL (lower left) and 1 μg/mL (lower right) of CHP were visualized using phase contrast microscopy. Original magnification, x100 (B) Representative confocal images of FN and pHDAC3 staining in rTGF-β-treated HPMCs (magnification, x200). (C) mRNA expression of FN, COL1A, αSMA, Bax, p53, p21, pHDAC3, and FOXM1 in the control, rTGF-β, and rTGF-β with CHP-treated HPMCs. Error bars represent standard error. (D) Representative blots and quantitative analysis of band intensities from Western blot analysis for FN, p53, HDAC3, and pHDAC3. ns, not significant, * $p < .05$, ** $p < .01$, and *** $p < .001$. FN, fibronectin; Col1A, type 1 collagen; αSMA, alpha-smooth muscle actin; Bax, Bcl-2 Associated X-protein; pHDAC3, phospho-histone deacetylase 3; FOXM1, forkhead box protein M1.

dialysis patients according to their CHP levels, no statistical difference was observed in age, sex, dialysis duration, and blood laboratory values between the groups with high and low CHP (Table S2). However, we discovered a significantly higher peritoneal Kt/V, which represents the adequacy of dialysis, in the high CHP group compared to the low CHP group ($p = .034$, Figure 7). This finding suggests that higher levels of CHP in peritoneal fluid may contribute to improved dialysis efficacy.

4 | DISCUSSION

The present study aimed to investigate the effect of CHP on PF in a murine model and explore the underlying mechanisms. The results demonstrated several important findings regarding the role of CHP in attenuating PF and its impact on inflammatory and fibrotic pathways, as well as mitochondrial functions.

CHP is a cyclic dipeptide which may be generated from TRH or endogenously synthesized de novo.^{18,37} CHP has

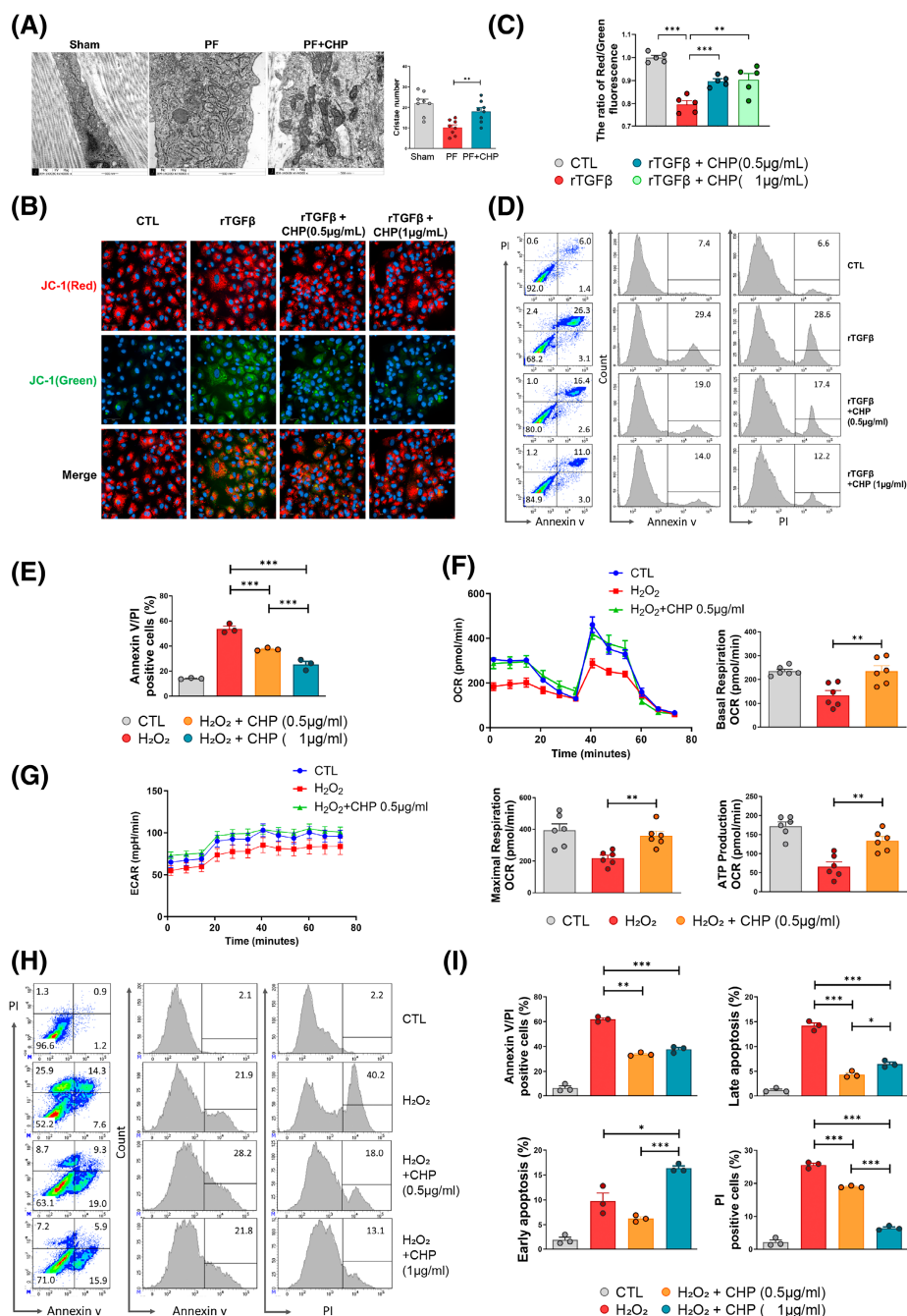


FIGURE 6 Mitochondrial function and apoptosis related to peritoneal fibrosis and oxidative stress were diminished with CHP.

(A) Transmission electron micrographs of mitochondria in PF and PF + CHP. Damaged mitochondria with matrix swelling and collapsed cristae were noted in PF and the morphology was restored in PF + CHP. Bar plot represents number of viable cristae in each group. ** $p < .01$

(B, C) Effect of CHP on mitochondrial membrane potential in response to fibrotic injury, as revealed by JC-1 staining. (B) Representative images following JC-1 staining. (C) Statistical data for the fluorescence intensities determined by JC-1 staining. The membrane potential is represented as the ratio of red to green fluorescence. ** $p < .01$ and *** $p < .001$.

(D) Representative flow cytometry images of Annexin V-FITC/PI staining and (E) quantitative analysis of apoptosis rates (Annexin V-FITC+/PI- and Annexin V-FITC+/PI+ cells). ** $p < .01$ and *** $p < .001$.

(F) Representative profiles and summarized data regarding oxygen consumption in HPMCs with H₂O₂. (Left) Real-time measurement of OCR in HPMCs. (Right) Bar plots represent calculated basal respiration OCR, maximal respiration OCR, and adenosine triphosphate production OCR.

(G) ECAR determined simultaneously with OCR in panel D.

(H) Representative flow cytometry images of Annexin V-FITC/PI staining and (I) quantitative analysis of early (Annexin V-FITC+/PI-) and late apoptosis (Annexin V-FITC+/PI+) and necrosis (Annexin V-FITC-/PI+) rates.

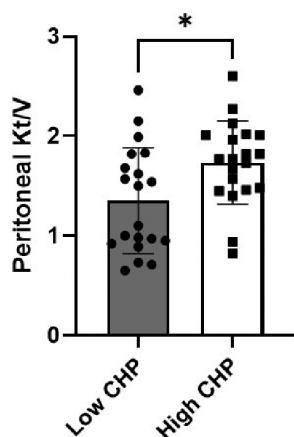


FIGURE 7 Association between peritoneal Kt/V and peritoneal CHP concentration. The x-axis represents two groups divided based on the median value of CHP concentration, indicating groups with high or low levels of CHP. The y-axis shows the peritoneal Kt/V values, which are indicative of the adequacy of peritoneal dialysis. An asterisk (*) indicates a statistically significant difference between the groups, with $p < .05$. Peritoneal Kt/V is a standard measure used to assess dialysis adequacy and is calculated using the following formula: $[\text{Dialysis urea}/\text{Plasma urea} \times \text{Dialysis Volume}] \times 7 \text{ days}/\text{Volume distribution of urea}$.

been found in the central nervous system, blood, gastrointestinal tract, and several body fluids.³⁸ There is growing evidence that CHP has its own unique receptors and biological functions in various organs.³⁹ In a previous study, CHP prevented oxidative stress and inhibited NF- κ B nuclear accumulation by activating the Nrf2/heme oxygenase-1 pathway in rat pheochromocytoma PC12 cells.¹⁹ In another study, CHP promoted insulin secretion, restoring inflammatory markers and the viability of pancreatic β -cells in diabetic rats.^{40,41} Furthermore, a recent study has demonstrated that CHP administration protects against the progression of liver fibrosis in mouse models of non-alcoholic fatty liver disease and steatohepatitis.²¹ In addition to the effects on the liver, our group recently discovered that administration of CHP may reduce ROS production and alleviate kidney fibrosis through the Nrf2-dependent pathway in chronic kidney injury models.¹⁶

Among the various effects of CHP, the present study focused on the anti-fibrotic effect of CHP. The prevention of PF is a major challenge to maintaining peritoneal dialysis because the progression of PF leads to a loss of ultrafiltration capacity and is the main reason that peritoneal dialysis is withdrawn.^{42,43} During the process of PF, key fibrogenic factors and specific downstream intracellular signal cascades, which include TGF- β and mitogen-activated protein kinase signal pathways, trigger the transcription of various profibrotic proteins.^{44–47} In this study, we found that PF led to the elevation of fibrosis markers, cell senescence, and mitochondrial injury

markers, suggesting various pathophysiological changes during PF. Interestingly, CHP treatment showed comprehensive and consistent recovery of these factors, both in vivo and in vitro. Recent studies have highlighted the crucial role of myeloid-derived cells in the pathogenesis of PF.^{48,49} These cells, including macrophages and dendritic cells, infiltrate the peritoneal cavity in response to inflammatory signals and contribute to the production of profibrotic factors, leading to the deposition of extracellular matrix components and fibrotic remodeling. The observed reduction in MDSCs in the spleen following CHP treatment has potential implications for PF. Given that MDSCs are known to contribute to the fibrotic process, a decrease in their systemic abundance may translate into a reduced infiltration of these cells into the peritoneal cavity.⁴⁸ Interestingly, we found that the proportion of three subsets of immature and mature myeloid cells was significantly reduced after being treated, even with a low dose of CHP (17.8 mg/kg). This reduction corresponded with a pronounced therapeutic effect on the progression of PF. This discovery may have significant implications for the management of PF.

HDAC3, the common upstream regulator we found in pathway analysis associated with PF and CHP treatment, is a class I HDAC which removes the acetyl moiety from histone tails resulting chromatin compaction.⁵⁰ According to previous research, HDACs modulate histone acetylation, chromatin condensation or relaxation, and transcriptional repression or activation.⁵¹ There are several studies that indicate that HDACs accelerate fibrogenesis and HDAC inhibitors regulate fibrosis.^{51,52} HDACs trigger secretion of profibrotic cytokines such as IL-1 β , IL-6, and TNF- α , which are crucial regulators of inflammation and fibrosis.⁵³ In a previous study, HDAC3 was shown to specifically promote TNF- α expression in response to LPS stimulation. Moreover, HDAC3 was identified as an inflammatory regulator in fibroblast-like synoviocytes in rheumatoid arthritis.⁵⁴ Furthermore, inhibition of HDAC could regulate fibrosis by reducing myofibroblast differentiation triggered by TGF- β as well as decreasing inflammatory cytokines.^{55,56} The present study showed results consistent with previous research, which found an association between fibrosis and HDAC in various organs. Our results suggest that the anti-inflammatory and antifibrotic effect of CHP may be related to the regulation of HDAC. Previous studies on CHP revealed that CHP acts through the NRF2 pathway.¹⁷ HDAC3 inhibition in diabetic mice activated NRF2 to prevent diabetic liver injury,⁵⁷ and alleviated type 2 diabetes mellitus-induced endothelial dysfunction through the NRF2 signaling pathway.⁵⁸ Further research into the function of HDAC3 in CHP activation is required.

Furthermore, we suggest that the mechanisms underlying the beneficial effects of CHP on PF is the potential

Activation of Nrf2 in peritoneum

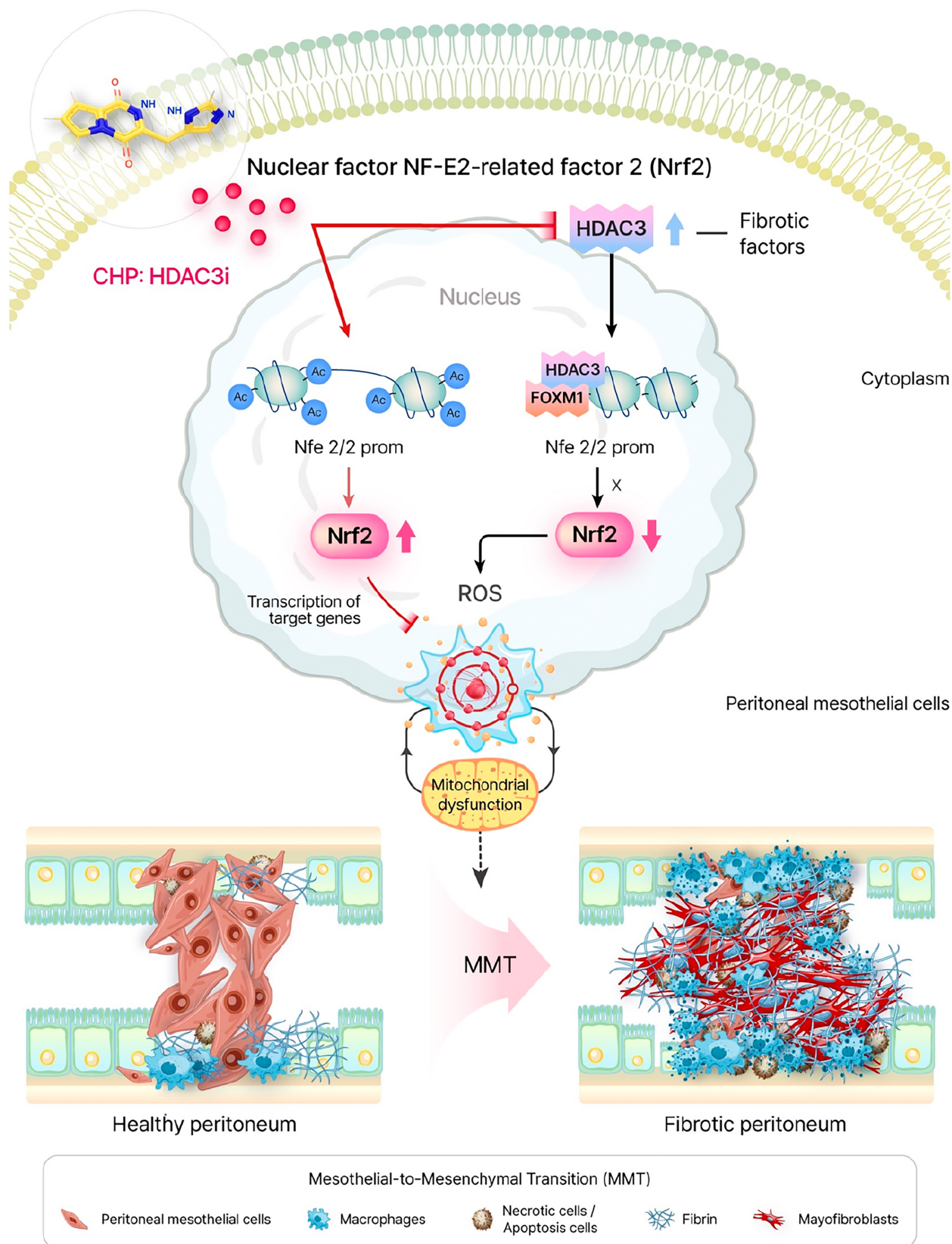


FIGURE 8 Working hypothesis of the potential links for CHP as a HDAC3 inhibitor to reduce peritoneal fibrosis. CHP blocks HDAC3 activity, leading to an increase in the transcription of Nrf2 which reduces oxidative stress associated with progressive peritoneal injury.

involvement of the Nrf2 and FOXM1 pathways, which are known to interact with HDAC3. Nrf2 is a transcription factor that plays a crucial role in cellular defense against oxidative stress and inflammation. Activation of Nrf2 can regulate the expression of antioxidant genes and other cytoprotective factors. Previous studies have demonstrated that HDAC3 inhibition can activate Nrf2 signaling, leading to protection against various pathological conditions.⁵⁸ For instance, in a study investigating endothelial dysfunction in type 2 diabetes mellitus, HDAC3 inhibition alleviated the dysfunction by activating the Nrf2 pathway.⁵⁷ This finding suggests that the protective effects of CHP on PF may involve the activation of Nrf2, which in turn promotes antioxidant defense and mitigates oxidative stress-induced damage. FOXM1 is a transcription factor that plays a critical role in cell cycle progression, proliferation, and differentiation. It has been implicated in various cellular processes, including fibrosis. Interestingly, previous studies have shown that FOXM1 interacts with HDAC3 and is involved in Nrf2-mediated redox regulation. In the context of fibrosis, the relationship between FOXM1 and HDAC3 has been observed in different organs and diseases. In a study focused on pulmonary fibrosis, inhibiting HDAC3 aberration mitigated fibrosis, which was accompanied by the repression of Nrf2.⁵⁹ This suggests that HDAC3 may regulate Nrf2 activity through the modulation of FOXM1. Similarly, in diabetic foot ulcers, the expression of multiple HDACs, including HDAC3, correlated with NRF2-mediated redox regulation, indicating a potential interplay between HDAC3, Nrf2, and the regulation of oxidative stress in diabetic complications.⁶⁰

Considering our findings, it is reasonable to suggest that CHP may affect mesothelial-mesenchymal transition (MMT) and contribute to the overall regulation of the peritoneum by reducing oxidative stress through the activation of Nrf2 by regulating HDAC3 (Figure 8). Through its potential to inhibit MMT, CHP could potentially disrupt the transformation of mesothelial cells into fibroblast-like cells, thereby interfering with the process of fibrotic remodeling. However, further studies are needed to fully elucidate the precise mechanisms underlying the interaction among HDAC3, Nrf2, and FOXM1 in the context of PF and the therapeutic effects of CHP.

In addition to investigating the effects of CHP on PF, the study also explored the association between CHP levels in human peritoneal fluid and the adequacy of dialysis in the maintenance of dialysis patients. While no significant differences were observed in peritoneal membrane transport function or ultrafiltration, a trend toward an association between CHP concentration and peritoneal kt/V was noted. These findings highlight the need for further large-scale investigation to fully understand the clinical

implications of CHP levels in peritoneal fluid and their potential as a biomarker for dialysis adequacy.

Our study has some limitations. CG injection or rTGF- β administration as a fibrosis induction model in this study may not completely match with the mechanism of PF in clinical practice. However, CG injection has been verified as a model for inducing sclerosing encapsulated peritonitis, a severe complication of peritoneal dialysis, in a previous study.^{61–63} As it is difficult to reproduce the fibrosis characteristic of the human peritoneum by regular peritoneal dialysis using an in vivo model, CG injection in mice was the reasonable choice for this proteomic analysis.

5 | CONCLUSIONS

This study demonstrates that CHP has significant protective effects against PF through the modulation of HDAC3 expression and associated signaling pathways. Our findings indicate that CHP treatment effectively reduces fibrosis and inflammation markers, improves mitochondrial function, and alleviates oxidative stress in both in vivo and in vitro models. Furthermore, the regulation of HDAC3 and its interaction with NRF2 and FOXM1 appears to play a crucial role in the antifibrotic and antioxidant effects of CHP. These results suggest that CHP has potential as a therapeutic agent for preventing or treating PF in peritoneal dialysis patients. Future prospective human studies are essential to validate these findings and explore the clinical application of CHP in extending the duration and efficacy of peritoneal dialysis.

AUTHOR CONTRIBUTIONS

Ji Eun Kim, Dohyun Han, Kyu Hong Kim, and SHY conceived experiments and analyzed data. Hoe-Yune Jung and Seung Hee Yang directed and coordinated the project. All authors were involved in writing the paper and had final approval of the submitted and published versions.

ACKNOWLEDGMENTS

The biospecimens for this study were provided by the Seoul National University Hospital Human Biobank, a member of the Korea Biobank Network, which is supported by the Ministry of Health and Welfare. All samples derived from the National Biobank of Korea were obtained with informed consent under institutional review board-approved protocols.

FUNDING INFORMATION

This work was supported by the NovMetaPharma Co., Ltd. (Seoul, Korea) through grants to Seoul National University Hospital and Kidney Research Institute,

Seoul National University Medical Research Center Republic of Korea (Grant No. 0620190730, 0320190030, and 0411-20190075).

DISCLOSURES

HYJ is a board member of NovMetaPharma. All other authors confirm that there are no conflicts of interest.

DATA AVAILABILITY STATEMENT

MS-based proteomics data of all identified peptides and the protein list have been deposited in the ProteomeXchange Consortium (<http://proteomecentral.proteomexchange.org>) via the PRIDE partner repository: dataset identifier PXD037403.

ORCID

Ji Eun Kim  <https://orcid.org/0000-0003-3094-2229>
 Dohyun Han  <https://orcid.org/0000-0002-0841-1598>
 Kyu Hong Kim  <https://orcid.org/0000-0002-5027-4881>
 Areum Seo  <https://orcid.org/0000-0002-9410-6660>
 Jong Joo Moon  <https://orcid.org/0000-0003-1034-0837>
 Jin Seon Jeong  <https://orcid.org/0000-0001-8200-9735>
 Ji Hye Kim  <https://orcid.org/0000-0001-6966-3353>
 Eunjeong Kang  <https://orcid.org/0000-0002-2191-2784>
 Eunjin Bae  <https://orcid.org/0000-0001-6890-4725>
 Yong Chul Kim  <https://orcid.org/0000-0003-3215-8681>
 Jae Wook Lee  <https://orcid.org/0000-0003-0120-8164>
 Ran-hui Cha  <https://orcid.org/0000-0003-2783-2600>
 Dong Ki Kim  <https://orcid.org/0000-0002-5195-7852>
 Kook-Hwan Oh  <https://orcid.org/0000-0001-9525-2179>
 Yon Su Kim  <https://orcid.org/0000-0003-3091-2388>
 Hoe-Yune Jung  <https://orcid.org/0000-0003-1802-5428>
 Seung Hee Yang  <https://orcid.org/0000-0002-8575-6610>

REFERENCES

- Wong B, Ravani P, Oliver MJ, et al. Comparison of patient survival between hemodialysis and peritoneal dialysis among patients eligible for both modalities. *Am J Kidney Dis*. 2018;71:344-351.
- Teitelbaum I, Glickman J, Neu A, et al. KDOQI US commentary on the 2020 ISPD practice recommendations for prescribing high-quality goal-directed peritoneal dialysis. *Am J Kidney Dis*. 2021;77:157-171.
- Mehrotra R, Devuyst O, Davies SJ, Johnson DW. The current state of peritoneal dialysis. *J Am Soc Nephrol*. 2016;27:3238-3252.
- Szeto CC, Li PK. Peritoneal dialysis-associated peritonitis. *Clin J Am Soc Nephrol*. 2019;14:1100-1105.
- Margetts PJ, Bonniaud P. Basic mechanisms and clinical implications of peritoneal fibrosis. *Perit Dial Int*. 2003;23:530-541.
- Yang Y, Liu K, Liang Y, Chen Y, Chen Y, Gong Y. Histone acetyltransferase inhibitor C646 reverses epithelial to mesenchymal transition of human peritoneal mesothelial cells via blocking TGF-beta1/Smad3 signaling pathway in vitro. *Int J Clin Exp Pathol*. 2015;8:2746-2754.
- Plum J, Hermann S, Fussboller A, et al. Peritoneal sclerosis in peritoneal dialysis patients related to dialysis settings and peritoneal transport properties. *Kidney Int Suppl*. 2001;78:S42-S47.
- Devuyst O, Margetts PJ, Topley N. The pathophysiology of the peritoneal membrane. *J Am Soc Nephrol*. 2010;21:1077-1085.
- Simon F, Tapia P, Armisen R, et al. Human peritoneal mesothelial cell death induced by high-glucose hypertonic solution involves Ca(2+) and Na(+) ions and oxidative stress with the participation of PKC/NOX2 and PI3K/Akt pathways. *Front Physiol*. 2017;8:379.
- Hara K, Hamada C, Wakabayashi K, et al. Scavenging of reactive oxygen species by astaxanthin inhibits epithelial-mesenchymal transition in high glucose-stimulated mesothelial cells. *PLoS One*. 2017;12:e0184332.
- Shin HS, Ko J, Kim DA, et al. Metformin ameliorates the phenotype transition of peritoneal mesothelial cells and peritoneal fibrosis via a modulation of oxidative stress. *Sci Rep*. 2017;7:5690.
- Ko J, Kang HJ, Kim DA, et al. Paricalcitol attenuates TGF-beta1-induced phenotype transition of human peritoneal mesothelial cells (HPMCs) via modulation of oxidative stress and NLRP3 inflammasome. *FASEB J*. 2019;33:3035-3050.
- Lopez-Armada MJ, Riveiro-Naveira RR, Vaamonde-Garcia C, Valcarcel-Ares MN. Mitochondrial dysfunction and the inflammatory response. *Mitochondrion*. 2013;13:106-118.
- Ishibashi Y, Sugimoto T, Ichikawa Y, et al. Glucose dialysate induces mitochondrial DNA damage in peritoneal mesothelial cells. *Perit Dial Int*. 2002;22:11-21.
- Hung KY, Liu SY, Yang TC, Liao TL, Kao SH. High-dialysate-glucose-induced oxidative stress and mitochondrial-mediated apoptosis in human peritoneal mesothelial cells. *Oxidative Med Cell Longev*. 2014;2014:642793.
- Kim KH, Moon JJ, Jeong JS, et al. Abstract Type: Oral Abstract Submission No.: OR-1499 Cyclo(His-Pro) prevents against oxidative stress-induced renal injury through activating Nrf2-mediated pathway. 2019.
- Minelli A, Conte C, Grottelli S, Bellezza I, Cacciatore I, Bolanos JP. Cyclo(his-pro) promotes cytoprotection by activating Nrf2-mediated up-regulation of antioxidant defence. *J Cell Mol Med*. 2009;13:1149-1161.
- Grottelli S, Ferrari I, Pietrini G, Peirce MJ, Minelli A, Bellezza I. The role of Cyclo(his-pro) in neurodegeneration. *Int J Mol Sci*. 2016;17:1332.
- Minelli A, Grottelli S, Mierla A, Pinnen F, Cacciatore I, Bellezza I. Cyclo(his-pro) exerts anti-inflammatory effects by modulating NF-kappaB and Nrf2 signalling. *Int J Biochem Cell Biol*. 2012;44:525-535.
- Koo KB, Suh HJ, Ra KS, Choi JW. Protective effect of cyclo(his-pro) on streptozotocin-induced cytotoxicity and apoptosis in vitro. *J Microbiol Biotechnol*. 2011;21:218-227.
- De Masi A, Li X, Lee D, et al. Cyclo (his-pro): a further step in the management of steatohepatitis. *JHEP Rep*. 2023;5:100815.
- Lee KM, Lee H, Han D, et al. Combined the SMAC mimetic and BCL2 inhibitor sensitizes neoadjuvant chemotherapy by targeting necrosome complexes in tyrosine aminoacyl-tRNA synthase-positive breast cancer. *Breast Cancer Res*. 2020;22:130.
- Jang HN, Moon SJ, Jung KC, et al. Mass spectrometry-based proteomic discovery of prognostic biomarkers in adrenal cortical carcinoma. *Cancers (Basel)*. 2021;13:3890.
- Park J, Kim H, Kim SY, et al. In-depth blood proteome profiling analysis revealed distinct functional characteristics of plasma

- proteins between severe and non-severe COVID-19 patients. *Sci Rep*. 2020;10:22418.
25. Kim H, Woo J, Dan K, et al. Quantitative proteomics reveals knockdown of CD44 promotes proliferation and migration in Claudin-low MDA-MB-231 and Hs 578T breast cancer cell lines. *J Proteome Res*. 2021;20:3720-3733.
 26. Kim JH, Kim H, Dan K, et al. In-depth proteomic profiling captures subtype-specific features of craniopharyngiomas. *Sci Rep*. 2021;11:21206.
 27. Cox J, Mann M. MaxQuant enables high peptide identification rates, individualized p.p.b.-range mass accuracies and proteome-wide protein quantification. *Nat Biotechnol*. 2008;26:1367-1372.
 28. Cox J, Neuhauser N, Michalski A, Scheltema RA, Olsen JV, Mann M. Andromeda: a peptide search engine integrated into the MaxQuant environment. *J Proteome Res*. 2011;10:1794-1805.
 29. Cox J, Hein MY, Lubner CA, Paron I, Nagaraj N, Mann M. Accurate proteome-wide label-free quantification by delayed normalization and maximal peptide ratio extraction, termed MaxLFQ. *Mol Cell Proteomics*. 2014;13:2513-2526.
 30. Moon JJ, Choi Y, Kim KH, et al. Inhibiting transglutaminase 2 mediates kidney fibrosis via anti-apoptosis. *Biomedicine*. 2022;10:1345.
 31. Yu MY, Kim JE, Lee S, et al. Kruppel-like factor 15 is a key suppressor of podocyte fibrosis under rotational force-driven pressure. *Exp Cell Res*. 2020;386:111706.
 32. Kim YC, Kim KH, Lee S, et al. ST2 blockade mitigates peritoneal fibrosis induced by TGF-beta and high glucose. *J Cell Mol Med*. 2019;23:6872-6884.
 33. Tyanova S, Temu T, Sinitcyn P, et al. The Perseus computational platform for comprehensive analysis of (prote)omics data. *Nat Methods*. 2016;13:731-740.
 34. Kerr EC, Raveney BJ, Copland DA, Dick AD, Nicholson LB. Analysis of retinal cellular infiltrate in experimental autoimmune uveoretinitis reveals multiple regulatory cell populations. *J Autoimmun*. 2008;31:354-361.
 35. Haile LA, von Waselewski R, Gamrekashvili J, et al. Myeloid-derived suppressor cells in inflammatory bowel disease: a new immunoregulatory pathway. *Gastroenterology*. 2008;135:871-881, 881 e871-875.
 36. Makarenkova VP, Bansal V, Matta BM, Perez LA, Ochoa JB. CD11b+/gr-1+ myeloid suppressor cells cause T cell dysfunction after traumatic stress. *J Immunol*. 2006;176:2085-2094.
 37. Kow LM, Pfaff DW. The effects of the TRH metabolite cyclo(his-pro) and its analogs on feeding. *Pharmacol Biochem Behav*. 1991;38:359-364.
 38. Prasad C. Bioactive cyclic dipeptides. *Peptides*. 1995;16:151-164.
 39. Prasad C. Limited proteolysis and physiological regulation: an example from thyrotropin-releasing hormone metabolism. *Thyroid*. 1998;8:969-975.
 40. Song MK, Hwang IK, Rosenthal MJ, et al. Anti-hyperglycemic activity of zinc plus cyclo (his-pro) in genetically diabetic Goto-Kakizaki and aged rats. *Exp Biol Med (Maywood)*. 2003;228:1338-1345.
 41. Song MK, Rosenthal MJ, Hong S, et al. Synergistic antidiabetic activities of zinc, cyclo (his-pro), and arachidonic acid. *Metabolism*. 2001;50:53-59.
 42. Sampimon DE, Barreto DL, Coester AM, Struijk DG, Krediet RT. The value of osmotic conductance and free water transport in the prediction of encapsulating peritoneal sclerosis. *Adv Perit Dial*. 2014;30:21-26.
 43. Morelle J, Sow A, Hautem N, et al. Interstitial fibrosis restricts osmotic water transport in encapsulating peritoneal sclerosis. *J Am Soc Nephrol*. 2015;26:2521-2533.
 44. Zhou Q, Bajo MA, Del Peso G, Yu X, Selgas R. Preventing peritoneal membrane fibrosis in peritoneal dialysis patients. *Kidney Int*. 2016;90:515-524.
 45. Ksiazek K, Korybalska K, Jorres A, Witowski J. Accelerated senescence of human peritoneal mesothelial cells exposed to high glucose: the role of TGF-beta1. *Lab Invest*. 2007;87:345-356.
 46. Matsuo H, Tamura M, Kabashima N, et al. Prednisolone inhibits hyperosmolarity-induced expression of MCP-1 via NF-kappaB in peritoneal mesothelial cells. *Kidney Int*. 2006;69:736-746.
 47. Ha H, Yu MR, Lee HB. High glucose-induced PKC activation mediates TGF-beta 1 and fibronectin synthesis by peritoneal mesothelial cells. *Kidney Int*. 2001;59:463-470.
 48. Louwe PA, Badiola Gomez L, Webster H, et al. Recruited macrophages that colonize the post-inflammatory peritoneal niche convert into functionally divergent resident cells. *Nat Commun*. 2021;12:1770.
 49. Terri M, Trionfetti F, Montaldo C, et al. Mechanisms of peritoneal fibrosis: focus on immune cells-peritoneal stroma interactions. *Front Immunol*. 2021;12:607204.
 50. Mullican SE, Gaddis CA, Alenghat T, et al. Histone deacetylase 3 is an epigenomic brake in macrophage alternative activation. *Genes Dev*. 2011;25:2480-2488.
 51. Ning L, Rui X, Bo W, Qing G. The critical roles of histone deacetylase 3 in the pathogenesis of solid organ injury. *Cell Death Dis*. 2021;12:734.
 52. Liu N, Zhuang S. Treatment of chronic kidney diseases with histone deacetylase inhibitors. *Front Physiol*. 2015;6:121.
 53. Gatla HR, Muniraj N, Thevkar P, Yavvari S, Sukhvasi S, Makena MR. Regulation of chemokines and cytokines by histone deacetylases and an update on histone deacetylase inhibitors in human diseases. *Int J Mol Sci*. 2019;20:1110.
 54. Angiolilli C, Kabala PA, Grabiec AM, et al. Histone deacetylase 3 regulates the inflammatory gene expression programme of rheumatoid arthritis fibroblast-like synoviocytes. *Ann Rheum Dis*. 2017;76:277-285.
 55. Frangogiannis N. Transforming growth factor-beta in tissue fibrosis. *J Exp Med*. 2020;217:e20190103.
 56. Chen F, Gao Q, Wei A, et al. Histone deacetylase 3 aberration inhibits klotho transcription and promotes renal fibrosis. *Cell Death Differ*. 2021;28:1001-1012.
 57. Zhang J, Xu Z, Gu J, et al. HDAC3 inhibition in diabetic mice may activate Nrf2 preventing diabetes-induced liver damage and FGF21 synthesis and secretion leading to aortic protection. *Am J Physiol Endocrinol Metab*. 2018;315:E150-E162.
 58. Huang S, Chen G, Sun J, et al. Histone deacetylase 3 inhibition alleviates type 2 diabetes mellitus-induced endothelial dysfunction via Nrf2. *Cell Commun Signal*. 2021;19:35.
 59. Chen F, Gao Q, Zhang L, Ding Y, Wang H, Cao W. Inhibiting HDAC3 (histone deacetylase 3) aberration and the resultant Nrf2 (nuclear factor erythroid-derived 2-related Factor-2) repression mitigates pulmonary fibrosis. *Hypertension*. 2021;78:e15-e25.
 60. Teena R, Dhamodharan U, Ali D, Rajesh K, Ramkumar KM. Gene expression profiling of multiple histone deacetylases (HDAC) and its correlation with NRF2-mediated redox regulation in the pathogenesis of diabetic foot ulcers. *Biomolecules*. 2020;10:1466.

61. Chang MY, Wang HH, Chen LH, et al. A mice model of chlorhexidine gluconate-induced peritoneal damage. *J Vis Exp*. 2022;182.
62. Inoue H, Torigoe K, Torigoe M, et al. Mitochondrial acid-5 ameliorates chlorhexidine gluconate-induced peritoneal fibrosis in mice. *Med Mol Morphol*. 2022;55:27-40.
63. Ishii Y, Sawada T, Shimizu A, et al. An experimental sclerosing encapsulating peritonitis model in mice. *Nephrol Dial Transplant*. 2001;16:1262-1266.

SUPPORTING INFORMATION

Additional supporting information can be found online in the Supporting Information section at the end of this article.

How to cite this article: Kim JE, Han D, Kim KH, et al. Protective effect of Cyclo(His-Pro) on peritoneal fibrosis through regulation of HDAC3 expression. *The FASEB Journal*. 2024;38:e23819. doi:[10.1096/fj.202400854R](https://doi.org/10.1096/fj.202400854R)